Axial interactions in the mixed-valent Cu_A active site and role of the axial methionine in electron transfer

Ming-Li Tsai[a], Ryan G. Hadt[a], Nicholas M. Marshall[b], Tiffany D. Wilson[b], Yi Lu[b,1], and Edward I. Solomon[a,1]

[a]Department of Chemistry, Stanford University, Stanford, CA 94305; and [b]Department of Chemistry, University of Illinois, Urbana, IL 61801

Contributed by Edward I. Solomon, July 30, 2013 (sent for review May 31, 2013)

Within Cu-containing electron transfer active sites, the role of the axial ligand in type 1 sites is well defined, yet its role in the binuclear mixed-valent Cu_A sites is less clear. Recently, the mutation of the axial Met to Leu in a Cu_A site engineered into azurin (Cu_A Az) was found to have a limited effect on E^0 relative to this mutation in blue copper (BC). Detailed low-temperature absorption and magnetic circular dichroism, resonance Raman, and electron paramagnetic resonance studies on Cu_A Az (WT) and its M123X (X = Q, L, H) axial ligand variants indicated stronger axial ligation in M123L/H. Spectroscopically validated density functional theory calculations show that the smaller ΔE^0 is attributed to H_2O coordination to the Cu center in the M123L mutant in Cu_A but not in the equivalent BC variant. The comparable stabilization energy of the oxidized over the reduced state in Cu_A and BC ($Cu_A \sim 180$ mV; BC ~ 250 mV) indicates that the S(Met) influences E^0 similarly in both. Electron delocalization over two Cu centers in Cu_A was found to minimize the Jahn–Teller distortion induced by the axial Met ligand and lower the inner-sphere reorganization energy. The Cu–S(Met) bond in oxidized Cu_A is weak (5.2 kcal/mol) but energetically similar to that of BC, which demonstrates that the protein matrix also serves an entatic role in keeping the Met bound to the active site to tune down E^0 while maintaining a low reorganization energy required for rapid electron transfer under physiological conditions.

spectroscopy | reduction potential | energy transduction pathway

Long-range electron transfer (ET) is vital to a wide range of biological processes, including two key energy transduction pathways essential for life: H_2O oxidation in photosynthesis and O_2 reduction in respiration (1, 2). Nature has adapted a conserved cupredoxin fold motif (i.e., the Greek-key β barrel) to construct two evolutionarily linked, but structurally distinct Cu-containing ET proteins (3–5). These are the mononuclear type 1 (T1) or blue copper (BC) and binuclear purple Cu_A proteins. The first coordination sphere of the classic BC sites [e.g., plastocyanin (Pc) and azurin (Az)] consists of a trigonally distorted tetrahedral environment where Cu resides in an equatorial plane formed by one S(Cys) and two N(His) ligands and has an axial S (Met) ligand (Fig. 1*A*) (6, 7). The binuclear purple Cu_A site consists of two bridging S(Cys) ligands and two equatorial N (His) ligands as well as an axial polypeptide backbone carbonyl oxygen [O(Gln) on Cu_O] and an axial thioether sulfur [S(Met) on Cu_M] (Fig. 1*B*) (8–11). Both sites carry out rapid, efficient long-range ET with rates on the order of 10^3–10^5 s^{-1} (12, 13).

Although BC proteins use a Cu^+/Cu^{2+} redox couple, the binuclear Cu_A sites use a $(Cu^{1+}–Cu^{1+})/(Cu^{1.5+}–Cu^{1.5+})$ redox cycle. The oxidized form of Cu_A is mixed-valent (MV), with a highly covalent Cu_2S_2 core that gives rise to its unique spectroscopic features. The unpaired electron is fully delocalized over the two Cu centers and exhibits a characteristic seven-line $^{63,65}Cu$ hyperfine splitting pattern in electron paramagnetic resonance (EPR) spectroscopy (14, 15). Maintaining valence delocalization even in the presence of a low symmetry protein environment has been attributed to the large electronic coupling (H_{AB}) resulting from a direct Cu–Cu σ bond and efficient superexchange facilitated by substantial Cu_2–$S(Cys)_2$ covalency. This strong electronic coupling between the two Cu's leads to a $\Psi \rightarrow \Psi^*$ (Cu–Cu $\sigma \rightarrow \sigma^*$) transition at ~13,500 cm^{-1} (16). Excitation into this transition using resonance Raman (RR) yields a large excited state distortion in the totally symmetric Cu_2S_2 core "accordion" mode (ν_1), a characteristic of Robin & Day class III MV delocalization (17–19). The two bridging S(Cys) ligands give rise to four in-plane S(p)-derived molecular orbitals (MOs) for S(Cys) $\rightarrow \Psi^*$ charge transfer (CT) transitions. These have been assigned to absorption bands in the region of 20,000 cm^{-1}. Laser excitation into these CT transitions gives rise to RR enhancement of three additional Cu_2S_2 core vibrations (*SI Appendix*, Fig. S1*A*). The functional advantage of a valence delocalization in terms of rapid, long-range ET at low driving forces (~45 mV) has been ascribed to lowering the reorganization energy (λ) by distributing structural rearrangements associated with redox over two Cu centers (20).

In nature, the S(Met) ligand of BC is sometimes found to be replaced by other protein residues. These can either coordinate to Cu [e.g., O(Gln) in stellacyanin (St)] or leave the axial position vacant (e.g., Leu in the fungal laccases) (21, 22). In BC, it was found that variation of the axial ligand from O(Gln) to S (Met) to nothing can tune E^0 over a 300 mV range (23). In nitrite reductase (NiR), the Cu^{2+}–S(Met) bond strength could be experimentally determined and was found to be weak (4.6 kcal/mol) as its loss is compensated by an increased S(Cys) donor interaction with Cu. The low strength of this bond suggested an important role of the protein in keeping the S(Met) ligand bound at physiological temperature. The contribution of the protein in stabilizing the active site structure has been referred to as an entatic/rack state in bioinorganic chemistry (24, 25). For BC sites, the protein matrix provides the negative free energy required to overcome the entropically favored S(Met) bond loss. This plays an important role in ET function as S(Met) binding stabilizes the oxidized more than the reduced state of the Cu site and lowers E^0 by ~200 mV.

Significance

Long-range electron transfer (ET) is vital in energy transduction pathways. Within metalloprotein ET active sites, the role of the axial ligand in the mononuclear, blue copper (BC), also called type 1 Cu, sites is well defined, whereas its role in the binuclear mixed-valent Cu_A sites is less clear. This study defines the axial interaction in the mixed-valent binuclear Cu_A active site and its role in ET. The axial S(Met) ligand is essential in tuning down the reduction potential while not increasing the inner-sphere reorganization energy, a similar role to that found for the S(Met) ligand in BC. Furthermore, much like BC, the S(Met) bond in Cu_A is weak and therefore under entatic control by the surrounding protein matrix.

Author contributions: M.-L.T., R.G.H., Y.L., and E.I.S. designed research; M.-L.T., R.G.H., N.M.M., and T.D.W. performed research; N.M.M., T.D.W., and Y.L. contributed new reagents/analytic tools; M.-L.T., R.G.H., Y.L., and E.I.S. analyzed data; and M.-L.T., R.G.H., and E.I.S. wrote the paper.

The authors declare no conflict of interest.

[1]To whom correspondence may be addressed. E-mail: edward.solomon@stanford.edu or yi-lu@Illinois.edu.

This article contains supporting information online at www.pnas.org/lookup/suppl/doi:10.1073/pnas.1314242110/-/DCSupplemental.

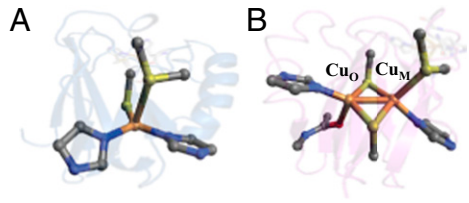

Fig. 1. The active sites of two previously published Cu ET proteins: (*A*) the monomeric T1 Cu Az from *Pseudomonas aeruginosa* (PDB ID code 4AZU) and (*B*) the binuclear purple Cu_A from *T. thermophilus* (PDB ID code 2CUA).

In contrast to BC proteins, S(Met) is the only axial ligand found in naturally occurring Cu_A sites [cytochrome *c* oxidase (CcO), nitrous oxide reductase (N_2OR), nitric oxide reductase (NOR), terminal oxidase in Sulfolobus acidocaldarius (SoxH)] (26). Interestingly, in contrast to BC, the Met to Leu mutation in the Cu_A Az only led to a 16 mV increase in E^0 (compared with an 86 mV increase for this mutant in BC Az) (27). This apparent difference in the extent of the axial ligand contribution to E^0 relative to previous studies on BC has led us to further explore its contribution to function in Cu_A and whether or not it is entatic as in BC. We use a combination of spectroscopic methods [low-temperature (LT) absorption and magnetic circular dichroism (MCD), RR, and EPR] coupled to density functional theory (DFT) calculations to investigate the geometric and electronic structures of Cu_A Az and a series of its axial ligand variants (M123X; X = Q, L, H). The influence of the axial ligand on the E^0 and λ are evaluated and compared with these properties in the well-understood BC site. Furthermore, the proposed involvement of Cu_A in ET pathways (28) as well as the entatic/rack nature of the Cu–S(Met) bond in Cu_A are evaluated and discussed.

Results

Spectroscopic Features of Axial Perturbations. The LT absorption and MCD data for WT Cu_A Az and its axial ligand variants are given in Fig. 2 *A* and *B* [see *SI Appendix*, Fig. S2 and Table S1 for simultaneous Gaussian resolutions of the LT absorption, MCD, and circular dichroism (CD)]. The LT absorption and MCD data have been previously assigned, and we follow those assignments here (16, 18). From low to high energy, bands 1, 4, 5, and 6 have been assigned as a $\Psi \rightarrow \Psi^*$ (Cu–Cu $\sigma \rightarrow \sigma^*$) transition and three S(Cys) → Cu ligand to metal charge transfer (LMCT) transitions, respectively. In going from WT (black) to M123Q (red), there are only minor changes in energies and intensities in the absorption and MCD spectra. However, for M123L (green) and M123H (blue), there is a redshift of band 1 (the $\Psi \rightarrow \Psi^*$ transition) and a decrease in intensity of band 4 relative to bands 5 and 6 in absorption and MCD [a S(Cys) → Cu CT transition].

The 77K RR data (λ_{ex} = 476.5 nm) in the 175–450 cm^{-1} region for WT Cu_A Az and its axial ligand variants are given in Fig. 2*C*. These show RR enhancement of the mixed Cu–S/Cu–N stretching mode (ν_2), the out-of-phase "twisting" Cu–S stretching mode (ν_3), and the Cu_2S_2 core breathing mode (ν_4) (29). The RR frequencies and intensities for M123Q (red) are very similar to WT Cu_A Az (black). However, both M123L and M123H show a decrease in the vibrational frequency of ν_2 and a decrease in the intensity of ν_3 relative to WT/M123Q.

The 77K X-band EPR data for Cu_A Az and its axial ligand variants are given in Fig. 2*D*. The spin Hamiltonian parameters are given in Table 1 (see *SI Appendix*, Fig. S3 and Table S2 for spectra and simulations). All show comparable hyperfine to both Cu's, consistent with complete delocalization. However, although $g_{||}$ for WT Cu_A Az and M123Q are similar and low ($g_{||}$ = 2.177 and 2.174 for WT and M123Q, respectively), $g_{||}$ for M123L and M123H increase to 2.215 and 2.255, respectively.

From these data, we group WT/M123Q into one class and M123H/M123L into another. The following five spectroscopic trends are observed in going from WT/M123Q to M123L/H: (*i*) a decrease in the relative intensity of the S(Cys) → Cu LMCT transitions (band 4 relative to bands 5 and 6), (*ii*) a redshift in the $\Psi \rightarrow \Psi^*$ transition (band 1), (*iii*) a decrease in intensity of ν_3, (*iv*) a decrease in the frequency of ν_2, and (*v*) an increase in $g_{||}$. In D_{2h} symmetry, the ground state of the Cu_A site is $^2B_{3u}$ (16). Four in-plane S(p) symmetry adapted linear combinations (SALCs) of the two bridged S(Cys) residues are predicted to give rise to two parity-allowed [$S(p_x)_g$ and $S(p_y)_g$] and two parity-forbidden [$S(p_x)_u$ and $S(p_y)_u$] S(Cys) → Ψ^* LMCT transitions (*SI Appendix*, Fig. S1B). In addition, in D_{2h}, the symmetry of ν_3 is B_{1g} and is

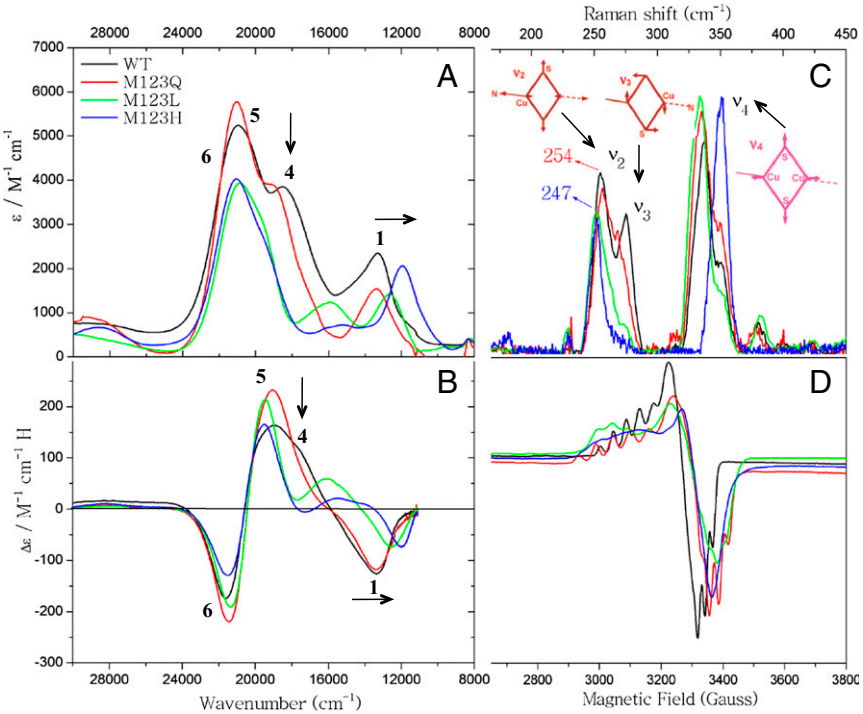

Fig. 2. Spectroscopic characterization of WT Cu_A Az and the M123X (X = Q, L, H) variants: (*A*) absorption spectra (10 K), (*B*) MCD spectra (10 K), (*C*) RR spectra (77 K, λ_{ex} = 476.5 nm), and (*D*) X-band EPR spectra (77 K).

Table 1. Experimental and calculated spin Hamiltonian parameters for WT Cu_A Az and the M123X (X = Q, L, H) variants

Axial variants	Exp. g_z	Exp. A_z^{Cu1}* (10^{-4}·cm^{-1})	Exp. A_z^{Cu2} (10^{-4}·cm^{-1})	Calc. g_z	Calc. A_z^{Cu1} (10^{-4}·cm^{-1})	Calc. A_z^{Cu2} (10^{-4}·cm^{-1})
WT	2.177	53	53	2.192	55	63
M123Q	2.174	61	57	2.190	60	68
M123L	2.215	35	35	2.209	48	59
M123H	2.255	58	42	2.214	52	55

*Note that the experimental A-values are approximate and dependent on the fit protocol. Results of two fits are given in *SI Appendix*, Fig. S3.

therefore not enhanced via an A-term intensity mechanism and must gain intensity through mixing with other totally symmetric (A_{1g}) modes. Thus, the decrease in intensity of the S(Cys) → Cu LMCT transition (band 4) in absorption and ν_3 in RR indicate that the active sites of M123L/H have higher effective symmetry than WT/M123Q. This eliminates mixing between parity-allowed and -forbidden SALC MOs as well as the mixing between the B_{1g} and energetically nearby A_{1g} modes in D_{2h} (*SI Appendix*, Fig. S1 *A* and *B*).

The $\Psi \rightarrow \Psi^*$ band in Cu_A has been described as a σ_g to σ_u^* transition. The energy separation between these MOs decreases upon weakening the Cu–Cu and Cu–N(His) bonds (i.e., a decrease in energy of the $\Psi \rightarrow \Psi^*$ transition). In addition, the EPR $g_{||}$-value has been correlated to the energy separation between the ground state, σ_u^*, and the low-lying π_u excited state (30). The $g_{||}$-value is given by:

$$g_{\|} = g_e + 8\xi_{3d}^{Cu}\alpha^2\beta^2/\Delta E, \quad [1]$$

where ξ is the spin-orbit coupling parameter for Cu^{2+}; α and β are the coefficients of Cu character in the σ_u^* and π_u orbitals, respectively; and ΔE is the energy separation between the π_u excited and the σ_u^* ground state. Therefore, the redshift of the $\Psi \rightarrow \Psi^*$ transition and the larger $g_{||}$-value in M123L/H both indicate that the Cu–Cu and Cu–N(His) bonds have weakened (the latter is also consistent with the lower frequency of the ν_2 vibrational mode in RR) relative to WT and its M123Q variant. These spectroscopic differences reflect the fact that M123L/H have stronger axial ligand interactions than WT and M123Q, which become comparable in strength to the relatively strong carbonyl backbone ligand on Cu_O. This increases the effective symmetry of M123L/H closer to D_{2h}, consistent with the decrease in intensity of the ν_3 vibration mode and the S(Cys) → Cu LMCT transition. Because Leu is a noncoordinating ligand, this would suggest its replacement with H_2O. Although His is a potentially good ligand, M123H is the only mutant that shows an additional pH dependence in EPR (pK_a ~6.5), indicating deprotonation of the axial His residue (*SI Appendix*, Fig. S4). We therefore assign the N(His) ligand as protonated and unbound at pH 5.5. Based on these spectroscopic trends for M123L and M123H (Fig. 2), H_2O is assigned as the axial ligand in both, whereas O(Gln) is weakly coordinated in M123Q. These models are evaluated below. Note that there are some quantitative differences in going from M123L to M123H. These include a lower energy $\Psi \rightarrow \Psi^*$ transition, a larger $g_{||}$-value, and a higher ν_4 vibrational frequency. These reflect a somewhat stronger axial H_2O interaction in M123H, which is supported by DFT calculations presented below.

Spectroscopically Validated DFT Structures. As a starting point for DFT calculations, a WT Cu_A Az model was constructed from the previously published 1.65 Å resolution X-ray structure [Protein Data Bank (PDB) ID code 1CC3] (*SI Appendix*, Fig. S5) (11). This model consists of the protein backbone loop connecting the two bridged S(Cys) residues as well as the equatorial His residues and both axial S(Met) and carbonyl backbone axial ligands to the Cu centers (93 total atoms). A partial geometry optimization was carried out with protein backbone and C_α constraints (see *SI Appendix*, Fig. S6 and Table S3 for structures and relevant optimized bond distances, respectively). This DFT optimized structure has a Cu–S(Met) distance of 2.95 Å, which agrees well with X-ray crystallography (2.98 Å) and previously reported DFT structures (18). The M123X (X = Q, L, H) variant structures for partial geometry optimization were constructed as indicated in *Materials and Methods*. For M123Q, O(Gln) is the axial ligand and remains at a long Cu–O distance [Cu–O(Gln), 4.18 Å].

For the M123L and M123H models, based on the above spectroscopic characterizations, H_2O was placed near the Cu_M center to serve as the axial ligand. The optimized M123L/H structures have shorter Cu–L_{axial} distances than those in WT/M123Q [Cu–O(H_2O) in M123L, 2.59 Å; Cu–O(H_2O) in M123H, 2.36 Å; Cu–S_{Met}, 2.95 Å; Cu–O_{Gln}, 4.18 Å]. These structures were used for time-dependent DFT (TD-DFT) calculations. The calculated absorption spectra are given in Fig. 3. These reasonably reproduce the experimentally observed trends in Fig. 2*A*. Specifically, in going from WT/M123Q to M123L/H, the calculations show a decrease in intensity of the S(Cys) → Cu LMCT transition (~18,000 cm^{-1}) and a redshift of the $\Psi \rightarrow \Psi^*$ transition (~12,000 cm^{-1}) as indicated by the arrows in Fig. 3. In addition, the calculated EPR parameters follow the experimentally observed trend: M123L/H both have larger calculated $g_{||}$-values than WT and M123Q (Table 1). This trend in the calculated $g_{||}$-value correlates reasonably to the calculated energy separation between the σ_u^* and π_u states (from TD-DFT) and the calculated Cu character in these orbitals (using Eq. **1**; *SI Appendix*, Table S5). Specifically, both M123L and M123H have smaller calculated σ_u^*/π_u energy separations and larger $g_{||}$-values.

In summary, the DFT structures of WT Cu_A Az and its M123X variants reproduce the spectroscopic trends and support H_2O binding as an axial ligand to the Cu_A core in the M123L/H variants and that S(Met) and O(Gln) are both relatively weakly interacting axial ligands in WT/M123Q, respectively. [Note we have also computationally evaluated possible Cu–O(H_2O) vibration modes for M123L. The stretch mixed into several modes at ~100 cm^{-1} and there is no significant calculated isotope shift for any of the resonance-enhanced ν2–ν4 vibrations (*SI Appendix*, Table S4)]. These structures are used below to evaluate the axial S(Met) ligand contributions to function in Cu_A relative to BC.

Analysis

Axial Ligand Influence on E^0. It has been previously reported that axial ligand variation in Cu_A azurin results in little change in E^0 (27). This is in contrast to the much larger E^0 changes for the analogous axial ligand mutations in BC. The smaller change in E^0 for the Cu_A variants, and thus the potentially diminished influence of the S(Met) axial ligand, was attributed to the nature of the diamond core in the Cu_A center. To further understand the effects of axial ligand binding to Cu_A on modulating E^0, we have

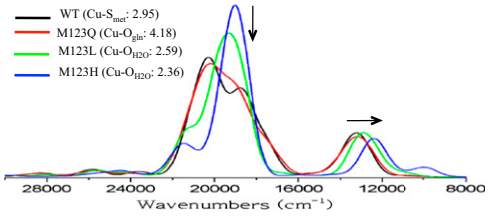

Fig. 3. TD-DFT calculated absorption spectra of WT Cu_A Az and M123X (X = Q, L, H) models. The Gaussian-broadened spectra were simulated using the SWizard program with Gaussian bandshapes that have full-width at half maxima of 1,350 cm^{-1} (from fits to LT absorption spectra).

Table 2. Experimental and calculated Cu–S(Met) bond strengths in BC, delocalized, and localized Cu_A sites

Model*	Blue copper	Deloclized Cu_A (Cu_O–Cu_M)	Localized Cu_A (Zn_O–Cu_M)
Exp†	4.6	n.d.	n.d.
Reduced‡	1.8	1.1	4.6
Oxidized§	7.5	5.2	16.8
ΔΔE(ox-red)	5.7	4.1	12.2

*Constrained Met residue replaced by dimethyl thioether.
†kcal/mol.
‡Energies are relative to a 10 Å Cu_M–S(thioether) distance. For Cu^+ BC $d_{Cu-S(thioether)-red}$ is fixed at $d_{Cu-S(thioether)-ox}$.
§Energies are obtained the same way as Cu^+ BC.

calculated the ionization energies (IEs) of WT, Met to Leu, and H_2O-bound DFT models of both BC (as a reference performed in the same manner) and Cu_A sites. Upon varying the axial ligand from S(Met) to Leu, the calculated IE increases by 130 and 100 mV for BC and Cu_A Az, respectively. For the BC model, this reflects the experimentally observed ΔE^0 (exp, 86 mV; calc., 130 mV). It is important to note that previous spectroscopic characterization of the Leu mutation in BC indicated that H_2O does not bind in the open axial ligand position (23, 31). In contrast, the experimental ΔE^0 in Cu_A Az is 20 mV, which is much smaller than the 100 mV increase calculated with no axial ligand. However, the calculated IE of the L-H_2O model only increases by 10 mV in Cu_A Az (20 mV for BC). This difference correlates well with the experimentally observed ΔE^0 (exp, 20 mV; calc., 10 mV) and is consistent with the spectroscopic assignment that H_2O coordinates to the Cu_A center in the M123L mutant. The calculated IEs for the series of WT, L, and L-H_2O models in both Cu_A Az and BC indicate that the small change in the experimental E^0 for M123L Cu_A relative to BC results from H_2O binding to the Cu center in Cu_A, and that, in Cu_A, the axial ligand should influence E^0 to an extent comparable to BC. Note that the changes in the calculated IE for the Met to Leu (without H_2O bound) mutation are quite similar for BC and Cu_A (BC, 130 mV; Cu_A, 100 mV) even though the redox states of the H_2O-bound Cu differ between the two active sites (Cu^+/Cu^{2+} for BC; $Cu^+/Cu^{1.5+}$ for Cu_A). We therefore explore contributions to this calculated difference in E^0 and evaluate the possibility of entatic control of the Cu–S(Met) bond by the protein environment in the Cu_A site relative to previous studies on BC.

Axial Met Bond Strength/Entatic State. For BC, the thermodynamic contributions to the Cu^{2+}–S(Met) bond have been determined experimentally ($\Delta H \sim 4.6$ kcal/mol). This indicated that the protein matrix and secondary environment in T1 Cu proteins can overcome the entropic gain of Cu–S(Met) bond rupture at physiological temperature. This is the entatic/rack state in T1 Cu proteins. Here, we use the experimental/computational results for parallel insight into Cu_A. The results of potential energy surface (PES) scans of Cu–S(Met) binding in Cu_A Az and BC (*SI Appendix*, Fig. S7) are compared in Table 2. The Cu^{2+}–S(Met) binding energy in BC is calculated to be 7.5 kcal/mol and agrees well with the previously calculated (6.8 kcal/mol) and experimental (4.6 kcal/mol) values (24). The S(Met) binding energy for $Cu_M^{1.5+}$ in Cu_A Az is calculated to be 5.2 kcal/mol, which is lower than BC, but not by half, which might be anticipated from the difference in oxidation state. The calculated Cu^{1+}–S(Met) bond strengths in BC and Cu_M^{1+} are similar (1.8 and 1.1 kcal/mol, respectively).

To explore how electron delocalization in the MV binuclear Cu_A core influences the stabilization energy of Cu–S(Met) bond in the same ligand environment, the Cu ion in the Cu_O site was replaced by Zn^{2+} to localize the unpaired electron on the Cu_M center (i.e., a [Zn^{2+}–Cu^{2+}] core). The calculated difference in stabilization energy of Cu_M–S(Met) bond between the reduced [Zn^{2+}–Cu^{1+}] (4.6 kcal/mol) and oxidized [Zn^{2+}–Cu^{2+}] (16.8 kcal/mol) cores is 12.2 kcal/mol. Note that the additional increase in Cu_M–S(Met) stabilization energy above twice that of the delocalized Cu_A core (4.1 kcal/mol) reflects the additional positive charge of Zn^{2+} compared with Cu^{1+}. [A parallel calculation with Ag^+ gives 5.9 kcal/mol. However, the ground state wavefunction contains some delocalization, which may lower the calculated bond strength relative to twice that of the Cu_A core (8.2 kcal/mol) (*SI Appendix*, Fig. S8).]

From the above calculations, the Cu–S(Met) bond in Cu_A is weak, yet is energetically similar to that in BC. The small binding energy of the Cu–S(Met) bond in Cu_A implies that the protein matrix in Cu_A also serves an entatic role in keeping the Met bound to the active site. Furthermore, the comparable stabilization energy of the oxidized over the reduced state between Cu_A and BC ($Cu_A \sim 180$ mV; BC ~ 250 mV, from the ΔΔE's in Table 2) indicates that the S(Met) likewise tunes down E^0 in Cu_A. Thus, the S(Met) does have a significant influence on E^0 even in the delocalized MV Cu_A site. The comparable function of the axial Met ligand on E^0 can be attributed to the different ligand sets between the Cu_A [two bridged S(Cys) and one equatorial N(His) for each Cu] and BC [one equatorial S(Cys) and two equatorial N(His)] sites.

Reorganization Energy. Maintaining a low reorganization energy (λ) is an important factor allowing the BC and Cu_A proteins to perform rapid long-range ET. The total reorganization energy (λ_T) of the ET process has inner-sphere and outer-sphere components (λ_i and λ_o, respectively). λ_T of engineered Cu_A Az has been determined to be roughly half that of BC Az (0.8 vs. 0.4 eV). This difference results in a threefold faster k_{ET} in Cu_A Az relative to BC (250 s^{-1} for BC and 650 s^{-1} for Cu_A) (32). It has been proposed that both λ_i and λ_o are lowered in Cu_A relative to BC due to electron delocalization in the MV Cu_2S_2 core and its larger charge radius relative to the mononuclear BC site (16, 33, 34). Here, we investigate the influence of the axial ligand and charge delocalization on the calculated λ_i relative to BC. The results of these calculations are summarized in Table 3. λ_i of the Cu_A Az and BC DFT models [both with an axial S(Met) ligand] are calculated to be 0.33 and 0.38 eV, respectively. These numbers are in agreement with previously reported values (18, 35–37). Upon removal of the axial S(Met) ligand, the calculated λ_i for both Cu_A Az and BC do not change (0.32 and 0.38 eV, respectively). This is consistent with previous considerations for axial ligand variants in stellacyanin (23).

We next explore the role of electron delocalization on λ_i by comparing the calculated values for the electron-delocalized [$Cu^{1.5+}$–$Cu^{1.5+}$] and electron-localized [Zn^{2+}–Cu^{2+}] cores. Without the axial S(Met) ligand, the calculated λ_i increases to 0.60 eV upon electron localization, which is almost twice that of the [$Cu^{1.5+}$–$Cu^{1.5+}$] model (0.32 eV) and consistent with the idea that delocalization reduces λ_i by roughly half. Upon binding of the S(Met) ligand to the localized Cu^{2+} center, the calculated λ_i increases to 0.74 eV. This 0.14 eV increase is in contrast to the negligible effect of the axial S(Met) on λ_i for the electron-delocalized [$Cu^{1.5+}$–$Cu^{1.5+}$] core. This difference in the calculated λ_i in the localized model is related to differences in structural distortions upon redox. S(Met) binding in the [Zn^{2+}–Cu^{2+}] core induces a significant Jahn–Teller distortion, which can be quantified by comparing the change in the angle between the S(Met)–Cu–S_1(Cys) and N(His)–Cu–S_2(Cys) planes upon redox (4° and 13° for delocalized [$Cu^{1.5+}$–$Cu^{1.5+}$] and localized [Zn^{2+}–Cu^{2+}] cores, respectively) (*SI Appendix*, Fig. S9) (38). Together, these results indicate that, as in BC, the S(Met) ligand contributes very little to λ_i upon redox for Cu_A Az. Also, as previously suggested, electron delocalization reduces λ_i by roughly half relative to a charge-localized model. However, it is additionally found here that it keeps the site from undergoing a Jahn–Teller distortion upon oxidation, which would increase λ_i.

Table 3. Calculated λ_i with and without a thioether bound to Cu in BC, delocalized, and localized Cu_A sites

Binding modes	Blue copper, eV	Deloclized Cu_A (Cu_O–Cu_M), eV	Localized Cu_A (Zn_O–Cu_M), eV
On	0.38*	0.33	0.74
Off†	0.38	0.32	0.60

*$\lambda_i = (E_{g\,=\,ox} - E_{g\,=\,red})_{reduced} + (E_{g\,=\,red} - E_{g\,=\,ox})_{oxidized}$, where "g=ox" and "oxidized" are the oxidation state of the geometry and wave function, respectively.
†Cu–S(thioether) fixed at 10 Å.

ET Pathways. Ligand–metal covalency plays an important role in activating ET pathways and increasing k_{ET} through increased donor-acceptor coupling (H_{DA}) (33, 39–41). The nature of the ET pathways coupling the Cu_A active site with its donor and acceptor has been the subject of much research. Recently, an alternative ET pathway for electron uptake from cytochrome c_{552} by the Cu_A site in *Thermus thermophilus* ba3 oxidase through the axial S(Met) ligand has been proposed (28). This involves a low-lying π_u excited state, which has an estimated 10% axial S(Met) character in the highest occupied molecular orbital (HOMO). Here, we explore the possible S(Met) contribution to an ET pathway. The β-lowest unoccupied molecular orbitals (LUMOs) of the σ_u^* ground state and the π_u excited state are given in Fig. 4 *A* and *B*, respectively. (Note that the π_u excited state was obtained by exchanging the electron occupation between σ_u^* and π_u orbitals in the σ_u^* optimized structure followed by optimization of the SCF density.) For both σ_u^* and π_u wavefunctions, no S(Met) character is observed. We further explored the possibility of S(Met) contribution to redox for both σ_u^* and π_u wavefunctions using electron density difference maps (EDDMs) between the reduced and oxidized optimized total electron densities (Fig. 4 *C* and *D*). The EDDM contour plots for both σ_u^* and π_u states are qualitatively similar to the corresponding β-LUMOs. Importantly, as with the β-LUMOs, the EDDMs have no S(Met) character. We note that there is a predominantly S(Met)-based b_1 orbital [HOMO-1, 42% S(p)(Met) character] that mixes into the HOMO [7% S(p)(Met) character] due to their close proximity in energy (*SI Appendix*, Fig. S10). This, however, involves two occupied levels and does not contribute to net bonding. Therefore, the previously reported 10% axial S(Met) character in the HOMO orbital appears to be a result of this occupied orbital mixing. We can therefore rule out the possibility that the axial S(Met) is a viable ET pathway in either the π_u excited and σ_u^* ground state.

Above we considered the electronic structure of the π_u excited state in the optimized σ_u^* ground state structure; the geometric changes related to the π_u excited state are now evaluated. We had previously found that elongation of the Cu–Cu bond results in a structure with a π_u ground state that is ~300 cm^{-1} higher in energy than the corresponding σ_u^* ground state structure (30). Recently, other structural coordinates have been emphasized (28). To further explore structural contributions that could lead to stabilization of either a σ_u^* or π_u state, a series of geometrically perturbed Cu_A structures have been taken as starting points for geometry optimizations (*SI Appendix*, Fig. S11). These distortions include: (*i*) the Cu–Cu distance (from 2.5 to 3.2 Å), (*ii*) the Cu–S(Cys)–Cu–S(Cys) dihedral angle (from 0 to 30°), (*iii*) the N(His)–Cu–Cu–N(His) dihedral angle (from –180 to –150°), (*iv*) distortion of the [Cu_2S_2] core along the accordion mode (ν_1), (*v*) elongation of the Cu–N(His) bonds, and (*vi*) elongation of the Cu–S(Cys) bonds. These distortions sample a large fraction of the Cu_A active site PES. All different starting structures optimized back to either the previously reported σ_u^* (Cu–Cu ~2.5 Å) or π_u (Cu–Cu ~3.1 Å) geometries. In addition, possible distortions of the π_u excited state relative to the σ_u^* ground state geometry were probed by monitoring the TD-DFT calculated σ_u^*/π_u energy change upon +/− displacements along normal modes (i.e., possible excited state distorting forces). The modes evaluated were taken from the frequency analysis of the Cu_A Az geometry [e.g., the Cu–Cu stretch (ν_{108}), the accordion distortion of the Cu_2S_2 core (ν_{154}), the N_{His}–Cu–Cu–N_{His} dihedral mode (ν_{161}), and the Cu–S_{Cys}–Cu–S_{Cys} dihedral mode (ν_{194})]. As shown in Fig. 4*E*, the slopes (and thus the degree of excited state distortion) of the two dihedral modes (ν_{161} and ν_{194}) are relatively flat compared with the normal modes associated with Cu–Cu elongation (ν_{108} and ν_{154}, both of which lower the energy of the π_u state by Cu–Cu elongation). The ground state optimizations and the magnitudes of excited state distorting forces indicate that Cu–Cu elongation is the preferential mode of distortion in the low-lying π_u excited state.

Discussion

From the above spectroscopic and computational results and analyses, the role of the axial S(Met) ligand in Cu_A is to tune down E^0 without significantly affecting λ_i. The contribution to lowering E^0 is especially important for Cu_A due to the narrow redox window (~90 mV) between Cu_A and its redox partners (i.e., cyt *c* for electron uptake and heme *a* for electron delivery in CcO). These functions of the axial ligand are similar to those in BC. Furthermore, the lack of S(Met) character in the EDDMs and β-LUMOs of either the σ_u^* ground state or the low-lying π_u excited state indicates that the S(Met) ligand is not involved in an ET pathway. This is supported by kinetic results on CcO from *Paracoccus denitrificans*, which show that the ET rate from cyt *c* to Cu_A is unperturbed by the axial Met to Ile mutation (42). The $Cu^{1.5+}$–S(Met) bond in Cu_A was calculated here to be weak and slightly weaker than the Cu^{2+}–S(Met) bond in BC (BC, 7.5 kcal/mol; Cu_A, 5.2 kcal/mol). This finding indicates that, much like BC, the surrounding protein matrix of the Cu_A active site must impose an entatic/rack state to overcome the entropically favored Cu–S(Met) bond rupture at physiological temperature.

Although the role of the axial Met in Cu_A is quite similar to BC, the binuclear Cu_A core has an intrinsic advantage relative to the mononuclear BC in terms of lowering λ_i and λ_o. The presence of

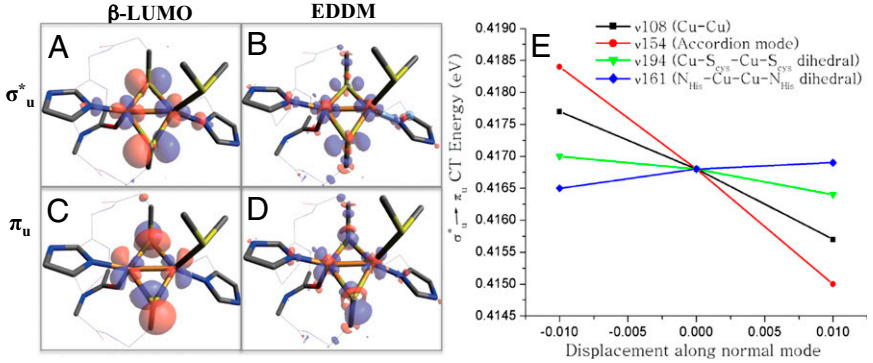

Fig. 4. The EDDMs and β-LUMOs of σ^*_u ground and π_u excited states in the σ^*_u optimized geometry (*A–D*) and the calculated π_u excited state slopes along normal modes ν_{108} (black), ν_{154} (red), ν_{194} (green), and ν_{161} (blue) (*E*).

two highly covalent Cu–S(Cys) bonds in Cu_A is also important for activating multiple ET pathways. In particular, the electron entry pathway to the Cu_A site needs to be efficient, as this active site is relatively buried in the protein matrix. This is in contrast to BC, where the electron entry point is a surface-exposed His ligand with little covalent character in the redox active molecular orbital. These factors facilitate rapid and efficient long-range ET with a low driving force (~45 mV) by the Cu_A active site.

In summary, a combination of LT absorption, MCD, RR, and EPR spectroscopies on WT Cu_A and its M123X (X = Q, L, H) axial ligand variants has demonstrated that Cu_2S_2 active cores in M123L/H are in a more symmetric environment. Spectroscopically validated DFT calculations indicate that the S(Met) ligand is essential in tuning down E^0 but not increasing λ_i, a similar role to that found for the S(Met) ligand in BC. The smaller experimental ΔE^0 for the Met to Leu mutation in Cu_A azurin relative to that in BC is not found to be a consequence of electron delocalization. Rather, this difference is attributed to the presence of a H_2O ligand in the M123L mutant of Cu_A, which is not present in the analogous mutant of BC. Furthermore, much like BC, the S(Met) bond to the active site in Cu_A is weak and therefore under entatic control by the surrounding protein matrix. This study demonstrates that a detailed spectroscopic characterization of metalloprotein active sites and their perturbed forms is imperative to provide molecular level insight into understanding geometric and electronic structure contributions to function.

Materials and Methods

Expression and purification of WT Cu_A Az and the variants studied here were performed using previously published protocols (27). UV-vis data were recorded in ammonium acetate buffer (pH 5.5) on a Cary 500 spectrophotometer. MCD was performed on Jasco J-730 and J-810 spectropolarimeters equipped with Oxford Instruments SM-4000 superconducting magnets. RR spectra were collected by detecting with an Andor Newton charge-coupled device detector cooled to –80 °C. Excitation was provided by a Coherent Innova Sabre 25/7 Ar^+ CW ion laser (476.5 nm, ~20 mW). EPR spectra were obtained by using a Bruker EMX spectrometer, ER 041 XG microwave bridge, and ER 4102ST cavity. DFT calculations were performed with Gaussian 03/09 and ORCA. For spectroscopic and computational details, see *SI Appendix*.

ACKNOWLEDGMENTS. This work was funded by National Science Foundation Grants CHE-0948211 (to E.I.S.) and CHE-1058959 (to Y.L.) and National Institutes of Health Grant DK-31450 (to E.I.S.). M.-L.T. received support from the Postdoctoral Research Abroad Program sponsored by the National Science Council, Taiwan (Republic of China), and R.G.H. acknowledges a Gerhard Casper Stanford Graduate Fellowship and the Achievement Rewards for College Scientists Foundation.

1. DeVault D, Parkes JH, Chance B (1967) Electron tunnelling in cytochromes. *Nature* 215(5101):642–644.
2. Ramirez BE, Malmström BG, Winkler JR, Gray HB (1995) The currents of life: The terminal electron-transfer complex of respiration. *Proc Natl Acad Sci USA* 92(26): 11949–11951.
3. Lu Y (2004) *Electron Transfer: Cupredoxins Biocoordination Chemistry, Comprehensive Chemistry II: From Biology to Nanotechnology*, eds McCleverty JA, Meyer TJ, Que LJ, Tolman WB (Elsevier, Oxford), Vol 8, pp 91–122.
4. Wilson TD, Savelieff MG, Nilges MJ, Marshall NM, Lu Y (2011) Kinetics of copper incorporation into a biosynthetic purple Cu(A) azurin: Characterization of red, blue, and a new intermediate species. *J Am Chem Soc* 133(51):20778–20792.
5. Chacón KN, Blackburn NJ (2012) Stable Cu(II) and Cu(I) mononuclear intermediates in the assembly of the Cu_A center of *Thermus thermophilus* cytochrome oxidase. *J Am Chem Soc* 134(39):16401–16412.
6. Guss JM, Freeman HC (1983) Structure of oxidized poplar plastocyanin at 1.6 A resolution. *J Mol Biol* 169(2):521–563.
7. Nar H, Messerschmidt A, Huber R, van de Kamp M, Canters GW (1991) Crystal structure analysis of oxidized *Pseudomonas aeruginosa* azurin at pH 5.5 and pH 9.0. A pH-induced conformational transition involves a peptide bond flip. *J Mol Biol* 221(3):765–772.
8. Iwata S, Ostermeier C, Ludwig B, Michel H (1995) Structure at 2.8 A resolution of cytochrome c oxidase from *Paracoccus denitrificans*. *Nature* 376(6542):660–669.
9. Williams PA, et al. (1999) The Cu_A domain of *Thermus thermophilus* ba_3-type cytochrome *c* oxidase at 1.6 A resolution. *Nat Struct Biol* 6(6):509–516.
10. Brown K, et al. (2000) Revisiting the catalytic Cu_Z cluster of nitrous oxide (N_2O) reductase. Evidence of a bridging inorganic sulfur. *J Biol Chem* 275(52):41133–41136.
11. Robinson H, et al. (1999) Structural basis of electron transfer modulation in the purple Cu_A center. *Biochemistry* 38(18):5677–5683.
12. Winkler JR, Malmström BG, Gray HB (1995) Rapid electron injection into multisite metalloproteins: Intramolecular electron transfer in cytochrome oxidase. *Biophys Chem* 54(3):199–209.
13. Solomon EI, et al. (1996) Electronic structure of the oxidized and reduced blue copper sites: Contributions to the electron transfer pathway, reduction potential, and geometry. *Inorg Chim Acta* 243(1):67–78.
14. Beinert H, Griffiths DE, Wharton DC, Sands RH (1962) Properties of the copper associated with cytochrome oxidase as studied by paramagnetic resonance spectroscopy. *J Biol Chem* 237(7):2337–2346.
15. Fee JA, et al. (1995) Multi-frequency EPR evidence for a binuclear Cu_A center in cytochrome *c* oxidase: Studies with a ^{63}Cu- and ^{65}Cu-enriched, soluble domain of the cytochrome ba_3 subunit II from *Thermus thermophilus*. *Biochem Biophys Res Commun* 212(1):77–83.
16. Gamelin DR, et al. (1998) Spectroscopy of mixed-valence Cu_A-type centers: Ligand-field control of ground-state properties related to electron transfer. *J Am Chem Soc* 120(21):5246–5263.
17. Wallace-Williams SE, et al. (1996) Far-red resonance raman study of copper A in subunit II of cytochrome *c* oxidase. *J Am Chem Soc* 118(16):3986–3987.
18. Xie X, et al. (2008) Perturbations to the geometric and electronic structure of the Cu_A site: Factors that influence delocalization and their contributions to electron transfer. *J Am Chem Soc* 130(15):5194–5205.
19. Robin MB, Day P (1968) Mixed valence chemistry–A Survey and Classification. *Advances in Inorganic Chemistry and Radiochemistry*, eds Emeleus HJ, Sharpe AG (Academic Press, New York and London), Vol 10, pp 247–422.
20. Solomon EI, Xie X, Dey A (2008) Mixed valent sites in biological electron transfer. *Chem Soc Rev* 37(4):623–638.
21. Hart PJ, et al. (1996) A missing link in cupredoxins: Crystal structure of cucumber stellacyanin at 1.6 A resolution. *Protein Sci* 5(11):2175–2183.
22. Germann UA, Muller G, Hunziker PE, Lerch K (1988) Characterization of two allelic forms of *neurospora crussa* laccase. *J Biol Chem* 263(2):885–896.
23. DeBeer George S, et al. (2003) Spectroscopic investigation of stellacyanin mutants: Axial ligand interactions at the blue copper site. *J Am Chem Soc* 125(37):11314–11328.
24. Ghosh S, et al. (2009) Thermodynamic equilibrium between blue and green copper sites and the role of the protein in controlling function. *Proc Natl Acad Sci USA* 106(13):4969–4974.
25. Gray HB, Malmström BG, Williams RJP (2000) Copper coordination in blue proteins. *J Biol Inorg Chem* 5(5):551–559.
26. Wilson TD, Yu Y, Lu Y (2013) Understanding copper-thiolate containing electron transfer centers by incorporation of unnatural amino acids and the Cu_A center into the type 1 copper protein azurin. *Coord Chem Rev* 257(1):260–276.
27. Hwang HJ, Berry SM, Nilges MJ, Lu Y (2005) Axial methionine has much less influence on reduction potentials in a Cu_A center than in a blue copper center. *J Am Chem Soc* 127(20):7274–7275.
28. Abriata LA, et al. (2012) Alternative ground states enable pathway switching in biological electron transfer. *Proc Natl Acad Sci USA* 109(43):17348–17353.
29. Andrew CR, et al. (1996) Identification and description of copper-thiolate vibrations in the dinuclear Cu_A site of cytochrome *c* oxidase. *J Am Chem Soc* 118(43): 10436–10445.
30. Gorelsky SI, Xie X, Chen Y, Fee JA, Solomon EI (2006) The two-state issue in the mixed-valence binuclear Cu_A center in cytochrome *C* oxidase and N_2O reductase. *J Am Chem Soc* 128(51):16452–16453.
31. Palmer AE, Randall DW, Xu F, Solomon EI (1999) Spectroscopic studies and electronic structure description of the high potential type 1 copper site in fungal laccase: Insight into the effect of the axial ligand. *J Am Chem Soc* 121(30):7138–7149.
32. Farver O, Lu Y, Ang MC, Pecht I (1999) Enhanced rate of intramolecular electron transfer in an engineered purple Cu_A azurin. *Proc Natl Acad Sci USA* 96(3):899–902.
33. DeBeer George S, et al. (2001) A quantitative description of the ground-state wave function of $Cu_{(A)}$ by X-ray absorption spectroscopy: Comparison to plastocyanin and relevance to electron transfer. *J Am Chem Soc* 123(24):5757–5767.
34. Hupp JT, Zhang XL (1995) Solvational barriers to interfacial electron transfer: Minimization via valence delocalization. *J Phys Chem* 99(3):853–855.
35. Hadt RG, Xie X, Pauleta SR, Moura I, Solomon EI (2012) Analysis of resonance Raman data on the blue copper site in pseudoazurin: Excited state π and σ charge transfer distortions and their relation to ground state reorganization energy. *J Inorg Biochem* 115:155–162.
36. Olsson MHM, Ryde U (2001) Geometry, reduction potential, and reorganization energy of the binuclear $Cu_{(A)}$ site, studied by density functional theory. *J Am Chem Soc* 123(32):7866–7876.
37. Olsson MHM, Ryde U, Roos BO (1998) Quantum chemical calculations of the reorganization energy of blue-copper proteins. *Protein Sci* 7(12):2659–2668.
38. LaCroix LB, et al. (1996) Electronic structure of the perturbed blue copper site in nitrite reductase: Spectroscopic properties, bonding, and implications for the entatic/rack state. *J Am Chem Soc* 118(33):7755–7768.
39. Beratan DN, Onuchic JN, Betts JN, Bowler BE, Gray HB (1990) Electron-tunneling pathways in ruthenated proteins. *J Am Chem Soc* 112(22):7915–7921.
40. Gurbiel RJ, et al. (1993) Detection of two histidyl ligands to Cu_A of cytochrome oxidase by 35-GHz ENDOR: $^{14,15}N$ and $^{63,65}Cu$ ENDOR studies of the Cu_A site in bovine heart cytochrome aa_3 and cytochromes caa_3 and ba_3 from *Thermus thermophilus*. *J Am Chem Soc* 115(23):10888–10894.
41. Lyons JA, et al. (2012) Structural insights into electron transfer in caa_3-type cytochrome oxidase. *Nature* 487(7408):514–518.
42. Zickermann V, et al. (1995) Perturbation of the Cu_A site in cytochrome-*c* oxidase of *Paracoccus denitrificans* by replacement of Met227 with isoleucine. *Eur J Biochem* 234(2):686–693.